In-situ and Ex-situ Investigations on Ternary Strategy and Co-solvents Effects towards High-Efficiency Organic Solar Cells

Ruijie Ma[1,6], Cenqi Yan[2,6], Patrick Wai-Keung Fong[2], Jiangsheng Yu[2], Heng Liu[3], Junli Yin[1], Jianhua Huang,[5] Xinhui Lu[3], He Yan*[1,4], Gang Li[2]*

[1]Department of Chemistry, Guangdong-Hong Kong-Macao Joint Laboratory of Optoelectronic and Magnetic Functional Materials, Energy Institute and Hong Kong Branch of Chinese National Engineering Research Center for Tissue Restoration & Reconstruction, Hong Kong University of Science and Technology, Clear Water Bay, Kowloon, Hong Kong, China
Email: hyan@ust.hk

[2]Department of Electronic and Information Engineering, Research Institute for Smart Energy (RISE), The Hong Kong Polytechnic University, Hung Hom, Kowloon, Hong Kong, China
Email: gang.w.li@polyu.edu.hk

[3]Department of Physics, Chinese University of Hong Kong, Hong Kong, New Territories Hong Kong, China

[4]Institute of Polymer Optoelectronic Materials and Devices, State Key Laboratory of Luminescent Materials and Devices, South China University of Technology (SCUT), Guangzhou, 510640 China

[5]College of Materials Science and Engineering, Huaqiao University, Xiamen,361021, China

[6]R. Ma and C. Yan contribute equally to this work.

Broader Context

Constructing ternary blend has now become one of the most popular tactics to uplift the power conversion efficiencies (PCEs) of organic solar cells (OSCs), which engenders the best single-junction OSC efficiencies to date. During the morphology study, the majority of the ternary work is focused on the interaction between the three materials and ignores the influence of the co-solvent on the ternary system. Herein, we carefully analyzed two ternary systems processed by two co-solvent systems by screening the film formation via a home-built time-resolved UV reflection/absorption setup. One binary host system is CB+DIO co-solvent processed PM6:eC9, the other is XY+PN non-halogenated co-solvent treated PM6:eC11. The amorphous polymer acceptor BN-T is chosen as the third component in these two systems. For the first time, we provide deep understanding on the role of co-solvent in achieving highly efficient ternary OSCs. As a result, 18.49% PCE of 18.49% is achieved by CB+DIO co-solvent processed PM6:eC9, and 18.02% for XY+PN. Notably, 18.02% is at the leading position for OSCs with non-halogenated main solvent and solvent additive for active layer. Furthermore, the 18.49% PCE is promoted to 18.96% by applying PEDOT:PSS modification, one of the highest values to date.

Abstract

The morphology of organic solar cells (OSCs) is a core topic for reaching ultimate photovoltaic performance. Herein, we focused on the combination of two important morphology regulation strategies – ternary strategy and cosolvent engineering. Using an amorphous polymer acceptor BN-T as the third component, the PM6:BTP-eC11 and PM6:eC9 host binary systems, treated by the respective (o-xylene and 1-phenylnaphthalene solvent system and chlorobenzene and1,8-diiodooctane solvent system,both realized effective improvement in the power conversion efficiencies (PCEs). However, ex-situ morphological characterizations revealed these two systems experienced different ways of change in phase segregation and molecular packing, which cannot be understood by the current popular miscibility analysis. In this work, in-situ investigation was carried out upon the spin cast and thermal annealing processes.

The time-resolved reflection spectroscopy technique showed that BN-T retained more PN in ternary films during the cast, thereby facilitating the eC11's aggregation, and enlarging its domain size. In contrast, BN-T's incorporation didn't affect the DIO's content in films, resulting in less separated morphology for eC9 based systems as predicted by the miscibility study. In addition to the state-of-the-art PCEs, this work provides an insightful understanding of the morphology evolution in ternary OSCs assisted by high-boiling solvent additive via in-situ investigation techniques.

Keywords: morphology, organic solar cells, ternary strategy, co-solvents, power conversion efficiency, time-resolved

Introduction

Solution-processed bulk-heterojunction organic solar cells (OSCs) have acquired > 18% power conversion efficiencies (PCEs) in various reports, thanks to the success of new materials and morphology optimization strategies.[1-15] Further efficiency gains are expected to be the result of a better understanding and more logical optimization of thin-film morphology, in parallel to new materials or interface engineering. To date, hundreds of photoactive materials have been produced with promising initial performance, and device engineering is very critical to unleash the materials' potential to reach desirable morphology and efficiency. Among the device engineering approaches, ternary-component strategy is the most popular topic in recent years.[16-35] Pursuing the favorable morphological evolution in the ternary system is at the core of optimizing any new OSC material towards excellent performance. As a result, one of the main goals of OSC research is to figure out the morphology tuning effect of ternary-component strategy. However, most research on high-performance ternary systems, focuses primarily on the interaction of the three component in active layer via ex-situ characterization.[36-38] The possible impacts of material-co-solvent interactions on the film formation are invisible in these studies. To fully understand the formation of ternary blend film, in-situ observation is a must, but synchrotron beamline enabled set-ups like in-situ GIWAXS/GISAXS are not easily available. Apart from comprehensive

investigation in binary film morphology, in-situ characterization can give more insights into ternary film.[39-44]

Here, we built ternary blends with BN-T (Poly[3,9-didodecyl-4,4,10,10-tetraphenyl-4,10-dihydrothieno[3',2':3,4][1,2]azaborolo[1,5-a]thieno[3',2':3,4][1,2]azaborolo[1,5-d]pyrazine-5,11-diium-4,10-diuide-co-2,5-thiophene]),[45] a polymer acceptor proven as amorphous in film (independently contributing none to crystallinity or phase separation), using two cutting-edge binary blends processed by different co-solvents: PM6 (poly[(2,6-(4,8-bis(5-(2-ethylhexyl)-4-fluorothiophen-2-yl)benzo[1,2-b:4,5-b']dithiophene))-co-(1,3-di(5-thiophene-2-yl)-5,7-bis(2-ethylhexyl)-benzo[1,2-c:4,5-c']dithiophene-4,8-dione):eC11 (2,2'-((2Z,2'Z)-((12,13-bis(2-butyloctyl)-3,9-diundecyl-12,13-dihydro-[1,2,5]thiadiazolo[3,4-]thieno[2",3":4',5']thieno[2',3':4,5]pyrrolo[3,2-g]thieno[2',3':4,5]thieno[3,2-b]indole-2,10-diyl)bis(methanylylidene))bis(5,6-dichloro-3-oxo-2,3-dihydro-1H-indene-2,1-diylidene))dimalononitrile) with ortho-xylene (XY) and 1-phenylnaphthalene (PN), and PM6:eC9 (2,2'- [[12,13-Bis(2-butyloctyl)-12,13-dihydro-3,9-dinonylbisthieno[2",3":4',5']thieno[2',3':4,5]pyrrolo[3,2-e:2',3'-g][2,1,3]benzothiadiazole-2,10-diyl]bis[methylidyne(5,6-chloro-3-oxo-1H-indene-2,1(3H)-diylidene)]]bis[propanedinitrile]) with chlorobenzene (CB) and 1,8-diiodooctane (DIO).[46-48] Since BN-T was proven effective to promote the PCE of PM6:PY-IT system (PY-IT is a polymerized small molecules bearing BTP core), we infer BN-T can also work with PM6:eC11 and PM6:eC9.[26] As a result, the efficiency of PM6:eC11:BN-T ternary devices increased to 18.10% from 17.15% in the binary counterpart, which is among the highest for OSCs processed by non-halogenated solvent(s) and non-halogenated solvent additive(s).

Meanwhile, the PCE of the PM6:eC9:BN-T ternary target was 18.49% (17.75% for the binary control) and further improved to 18.96% by a reported interface engineering. Both ternary OSCs were found at cutting-edge PCE levels, implying the importance of further morphological understanding based on them. We discovered that these two ternary blends took different morphology variation routes, for crystallinity and phase

separation issues. The miscibility analysis can explain the change in eC9-based ternary series, but it fails to explain the change in eC11-based ternary series, signaling that a separate factor took the lead in morphology formation. The addition of BN-T can contain more PN after spinning and create a more segregated phase distribution, according to the time-resolved reflectance measurement. PM6:eC9:BN-T films, on the other hand, exhibit no variations in solvent additive (DIO) retention, resulting in phase separation that is consistent with miscibility prediction alone. This work uses ternary designs to generate high-performance OSCs, provides in-depth morphological understandings, and provides a novel and instructive technique for studying the working mechanism of ternary systems.

Results and Discussion

Figure 1a displays the chemical structures of deployed photovoltaic materials, whereas **Figure 1b** depicts their energy level distribution as determined by cyclic voltammetry (CV) measurements (in **Figure S1**). PM6, eC11, eC9, and BN-T exhibit the highest occupied molecular orbital (HOMO) values of -5.55, -5.61, -5.70, and -5.60 eV, and the lowest unoccupied molecular orbital (LUMO) values of -3.54, -4.05, -4.02, and -3.62 eV, respectively. The energy levels of BN-T are well aligned with those of the host systems. **Figure S2a** shows the normalized UV-vis-NIR absorption spectra of XY+PN processed PM6, eC11, BN-T, and mixed acceptor-based films, and **Figure S2b** depicts those of CB+DIO processed PM6, eC9, and BN-T. When PM6 is treated with XY+PN and CB+DIO, its absorbance is very similar, suggesting that these two co-solvents have no effect on its aggregation capabilities. For BN-T, different absorption profiles have been discovered: The XY+PN processed BN-T film exhibits a lower 0-0 vibrational peak than the CB+DIO processed BN-T film, but a stronger 0-1 vibrational peak, indicating that H- aggregation is more prominent in the XY+PN cast film. The 0-0 vibrational peak of eC11 film processed by XY+PN is significant, surpassing the other two peaks for monomers and H- aggregates; however, the 0-1 peak of CB+DIO cast eC9 has the same order of intensity as the 0-0 peak, indicating that J- aggregation is less dominant.[49-50] Both eC11 (XY+PN) and eC9 (CB+DIO) demonstrate blue shift

absorption in BN-T integrated acceptors constructed films, which implies fewer J-aggregates after incorporating BN-T. These phenomena tell that BN-T could play a vital role in regulating the aggregation of both systems.

Figure 1c-d illustrate the absorption spectra of PM6:eC11:BN-T (1:1.2:0, 1:1.2:0.1, 1:1.2:0.2) film processed by XY and PN, and of PM6:eC9:BN-T (1:1.2:0, 1:1.2:0.1, 1:1.2:0.2) film processed by CB and DIO. It is observed incorporating BN-T increases the normal absorption of XY+PN treated films, suggesting the tuning effect is promoting the global aggregation of eC11. By comparison, PM6:eC9 (CB+DIO) has an excellent good balance of donor and acceptor absorption, signaling that its initial aggregation is good. Adding extra BN-T has negligible influence on the absorption profile, but it does increase the general aggregation of both PM6 and eC9.

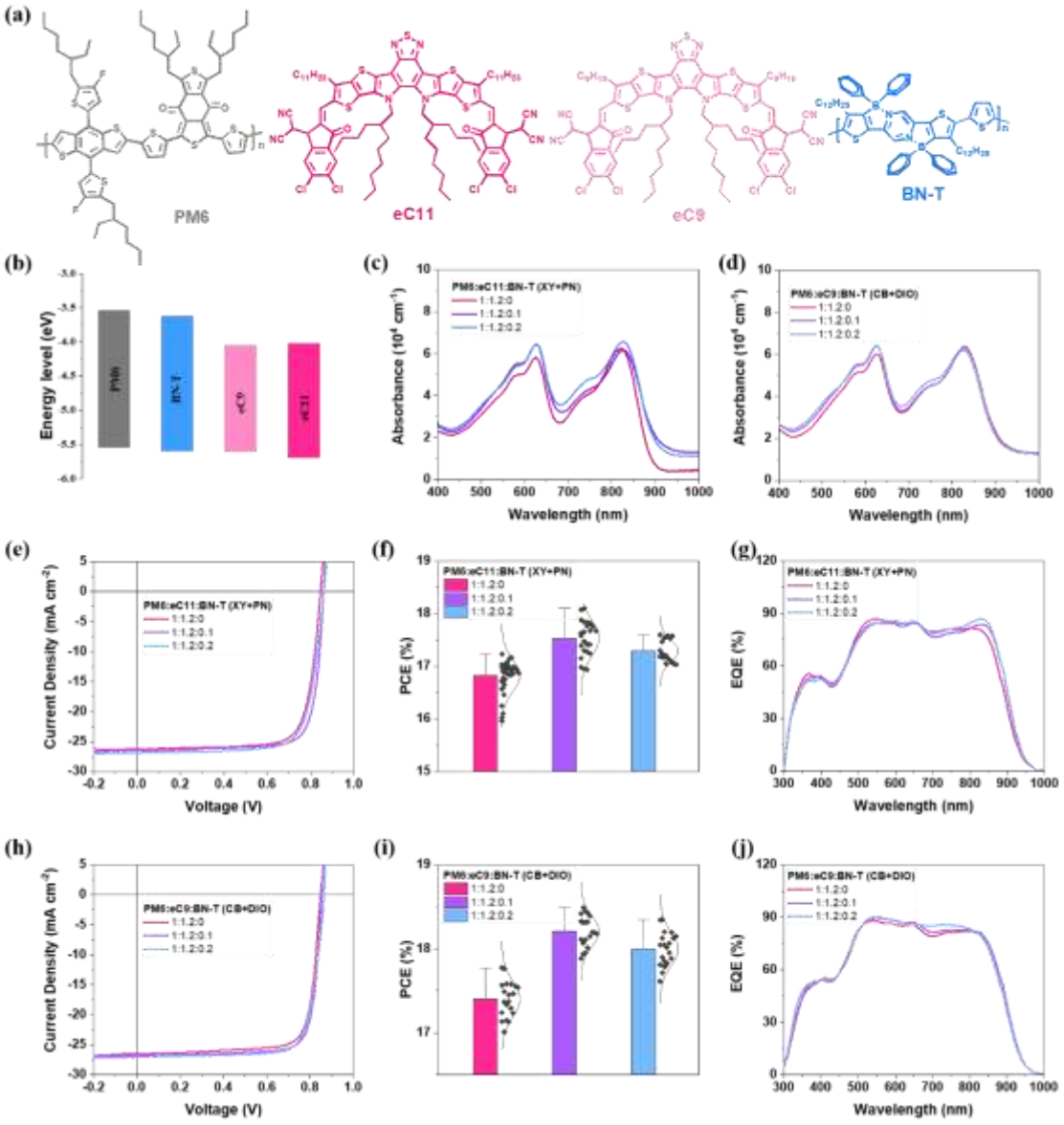

Figure 1. (a) Chemical structures and (b) Energy level distribution of PM6, BN-T, eC9 and eC11. UV-vis-NIR absorbance of (c) PM6:eC11:BN-T (XY+PN) and (d) PM6:eC9:BN-T (CB+DIO) films based on different weight ratios. (e) *J-V* curves, (f) PCE distributions and (g) EQE spectra of XY+PN co-solvent processed devices based on PM6:eC11:BN-T blends. (h) *J-V* curves, (i) PCE distributions and (j) EQE spectra of CB+DIO co-solvent processed devices based on PM6:eC9:BN-T blends.

After that, a series of binary and ternary solar cells were made to assess the influence of BN-T incorporation. The recipe was motivated by a recent study in which the PM6:BN-T blend demonstrated poor device performance, and thus BN-T was added to the host systems as a third component. The optimal proportions for ternary blends were found to be 1:1.2:0.1 for both PM6:eC11:BN-T (XY+PN) and PM6:eC9:BN-T

(CB+DIO) based devices, respectively. In comparison to the binary control system, the optimal PM6:eC11:BN-T-based solar cell exhibited simultaneously improved open-circuit voltage (V_{OC}), short-circuit current density (J_{SC}), fill factor (*FF*), and enhanced PCE from 17.15% to 18.02%. When the content of BN-T increases, the efficiency declines to 17.56%. Notably, the high PCE of 18.02% was achieved by using fully non-halogenated co-solvents (XY+PN), and is among the highest level for this type of OSCs. **Table S1** and **Figure S3a** summarized the efficiencies produced by pure non-halogenated solvent, a non-halogenated main solvent with halogenated solvent additive, and non-halogenated main solvent with non-halogenated solvent additive. Previous literatures have discussed the advantages of non-halogenated additives over their halogenated counterparts.[51-52] This brief comparison confirms that the performance obtained here is at the cutting-edge of current OSC research, making upcoming morphology analyses more meaningful. The optimal efficiency of CB+DIO co-solvent treated devices based on PM6:eC9:BN-T is 18.49%, not substantially better than 17.75% of the binary control, which supports the abovementioned hypothesis that morphological tuning effect of BN-T is not equally significant. **Table 1** lists all of the parameters, and **Figure 1e** and **1h** show the current density versus voltage (J-V) curves of the best device of each group. These best results were from at least 20 independent devices, as shown in **Figure 1f** and **1g**. In addition, interface engineering was utilized to further improve the PCE of this optimal system.[53] The *J-V* curves and EQE spectra are given in **Figure S3b and S3c**. As a consequence, the PCE is as high as 18.96%, which is able to compete the most advanced progresses of the OSC field.

Table 1. Device performances.

Systems	V_{OC} (V)	J_{SC} (mA cm^{-2})	*FF* (%)	PCE (%)
PM6:eC11:BN-T (XY+PN)				
1:1.2:0	0.846	26.23/25.60	77.3	17.15 (16.82±0.30)
1:1.2:0.1	0.856	26.54/26.05	79.3	18.02 (17.53±0.34)
1:1.2:0.2	0.860	26.91/26.52	75.9	17.56 (17.29±0.21)
PM6:eC9:BN-T (CB+DIO)				
1:1.2:0	0.849	26.53/26.31	78.8	17.75 (17.40±0.21)
1:1.2:0.1	0.859	26.84/26.65	80.2	18.49 (18.29±0.18)

1:1.2:0.2	0.863	27.06/26.74	78.1	18.24 (18.00±0.20)

The brackets contain averages and standard errors of PCEs based on at least 20 devices.

'The external quantum efficiency (EQE) of each system was tested to ensure the accuracy of the results. The integrated J_{SC} values are also shown in **Table 1** (after the slashes). The results suggest that the measured values are within 2.5% error. Furthermore, the EQE response for eC11's absorption peak is improved in ternary devices, compatible with optical observations. For eC9 based solar cells, the EQE spectra display very similar shapes, also consistent with previous measurements.

Then we performed device physics analyses to screen the change brought by BN-T. We performed photocurrent versus effective voltage (J_{ph} vs V_{eff}) and J_{SC} versus light intensity (J_{SC} vs P_{light}) characteristics for target and control systems. As shown in **Figure S4**, the charge separation and extraction display no distinct change among binary and ternary blends. The S values of PM6:eC11:BN-T are 0.986, 0.991, and 0.982 for 1:1.2:0, 1:1.2:0.1, and 1:1.2:0.2 weight ratios, respectively, indicating that bimolecular recombination is reduced in optimal ternary blend.These values are 0.989, 0.994 and 0.987 for PM6:eC9:BN-T systems with the ratio of 1:1.2:0, 1:1.2:0.1 and 1:1.2:0.2, respectively. The J_{SC} vs P_{light} relationships, however, are not meaningful here, because the trap-assisted recombination is thoroughly covered by bimolecular one at 1-sun illumination.

Next, we evaluated the mobilities of each active layer using the space charge limited current (SCLC) method. The fabrication steps for hole-only and electron-only devices are described in Supporting Information. The results for hole mobility (μ_h) and electron mobility (μ_e) are plotted in **Figure S5**. The derived μ_hs are 4.09×10^{-4}, 7.19×10^{-4}, and 6.26×10^{-4} $cm^2V^{-1}s^{-1}$ with the increase of BN-T in the XY+PN cast PM6:eC11 blend; and μ_es are 1.40×10^{-3}, 1.72×10^{-3} and 1.29×10^{-3} $cm^2V^{-1}s^{-1}$, respectively. The optimal one exhibits the most efficient and balanced charge transport. As for CB+DIO processed PM6:eC9:BN-T films, the (μ_h, μ_e) values for 1:1.2:0, 1:1.2:0.1 and 1:1.2:0.2 mass scale combinations are (4.00×10^{-4}, 14.1×10^{-4}), (6.34×10^{-4}, 17.5×10^{-4}) and (6.19×10^{-4}, 14.5×10^{-4}) $cm^2V^{-1}s^{-1}$, which demonstrates similar variation tendency.

Both optimized ternary blends exhibit more efficient and balanced charge transport compared with their binary counterparts, consistent with their superior performances and suppressed bimolecular recombination.

Subsequently, the existence of energy transfer and charge transfer between acceptors was investigated. Photoluminescence (PL) spectra of eC11:BN-T (XY) and eC9:BN-T(CB) films, were measured and devices based on acceptor(s) without the presence of PM6 were also fabricated. The results are summarized in **Figure S6**. It is suggested that slight energy transfer takes place from eC11 to BN-T in their XY cast films, and from eC9 to BN-T in CB cast layers. Charge transfer is also observed in both ternary blends. These results are in accordance with the previous reports.

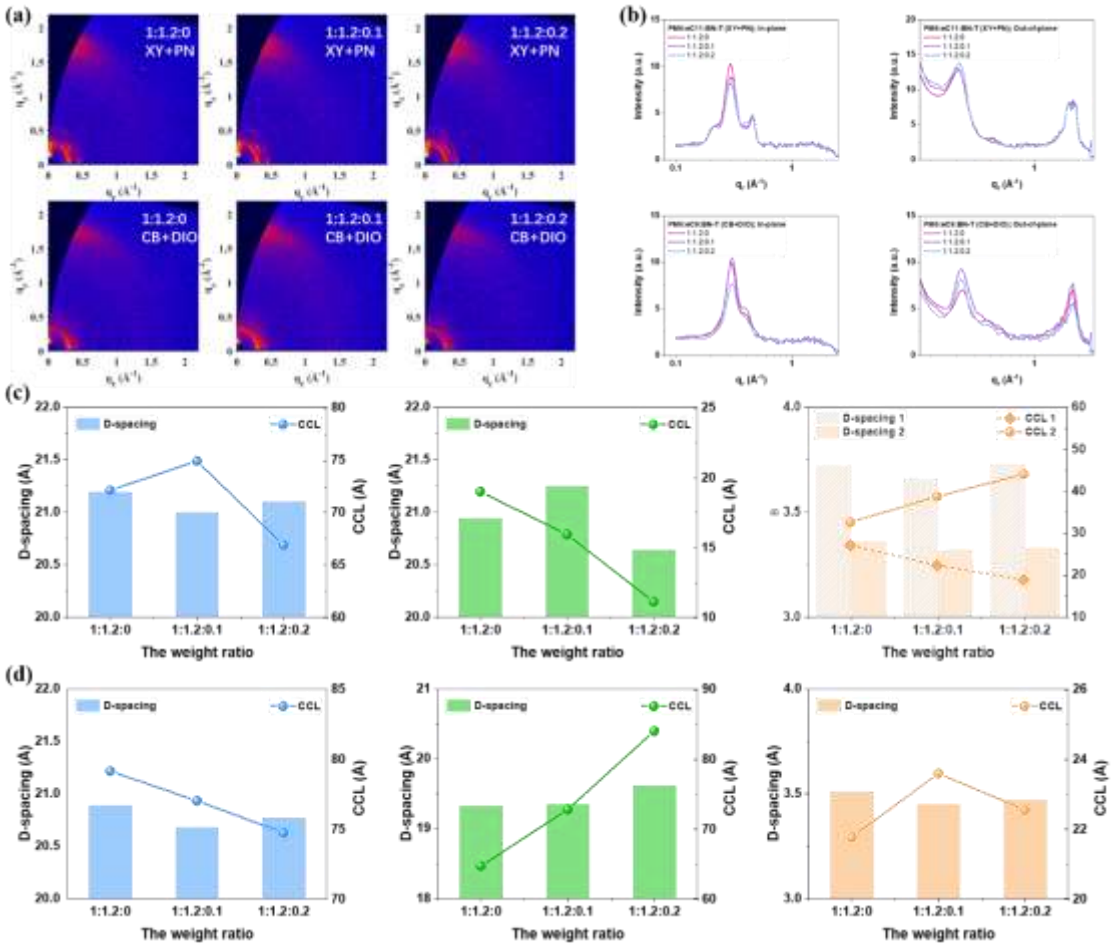

Figure 2. (a) 2D GIWAXS patterns and (b) In-plane and out-of-plane line-cuts for each system. (c) The d-spacing and CCL variation with the increase of BN-T's content in the XY+PN treated films: in-plane lamellar peak (blue); out-of-plane lamellar peak (green);

out-of-plane π-π peak. (d) The d-spacing and CCL variation with the increase of BN-T's content in the CB+DIO treated films: in-plane lamellar peak (blue); out-of-plane lamellar peak (green); out-of-plane π-π peak.As previously stated, ex-situ observations were first used to obtain basic information, as the morphology study is the basis of this work and also fundamentally required for understanding the device performances,

The grazing incidence wide-angle X-ray scattering (GIWAXS) experiments were utilized to investigate the molecular packing characteristics of each blend.[54-58] The 2D patterns and corresponding line cuts are shown in **Figures 2a-b**, while the calculated parameters are summarized in **Table S2-5**. The d-spacing and crystalline coherence length (CCL) values for both systems are also shown in **Figures 2c** and **2d**, to present the molecular packing variation. For XY+PN processed PM6:eC11:BN-T systems, increasing the content of BN-T does not affect the d-spacing for in-plane (IP) directional lamellar peaks, but PM6:eC11:BN-T with weight ratio of 1:1.1:0.1 exhibits the largest CCL. The out-of-plane (OOP) lamellar peaks also show no significant position shift, but CCLs continuously dropped with the increased proportion of BN-T.. The fitting results show two coupled π-π peaks along the OOP direction. The one with smaller d-spacing values exhibits CCLs increasing from 32.59 Å, to 38.75 Å and 44.06 Å. Because BN-T was previously proven to be amorphous, the lower lamellar packing crystallinity may be explained. However, the improved crystallinity for π-π peaks, as well as the variation in CCL of IP directional lamellar peaks, must be linked to BN-T in a more complicated way.

The packing change tendency in CB+DIO processed eC9 based blend films differs from that in XY+PN processed PM6:eC11:BN-T blend film. The IP lamellar peaks exhibit a slight drop in CCL values (79.17 Å, 77.05 Å, and 74.75 Å for 1:1.2:0, 1:1.2:0.1, and 1:1.2:0.2 ratios), and those of lamellar peaks of OOP direction rise from 64.74 Å to 72.84 Å and 84.09 Å. Besides, the OOP π-π peaks are located at 1.792 $Å^{-1}$, 1.824 $Å^{-1,}$ and 1.812 $Å^{-1}$ with CCLs of 21.77 Å, 23.60 Å, and 22.56 Å, for PM6:eC9:BN-T blends with weight ratios of 1:1.2:0, 1:1.2:0.1 and 1:1.2:0.2. The phenomenon here suggests that adding BN-T can enhance the face-on orientation, and subtly tune the crystallinity. The GIWAXS results for the two material systems processed by two co-

solvent combinations display very different changes. As a result, the morphological tuning impact of BN-T cannot be explained solely by investigating its interactions with host materials (PM6:eC11 or PM6:eC9), which is generally enabled by the miscibility study.

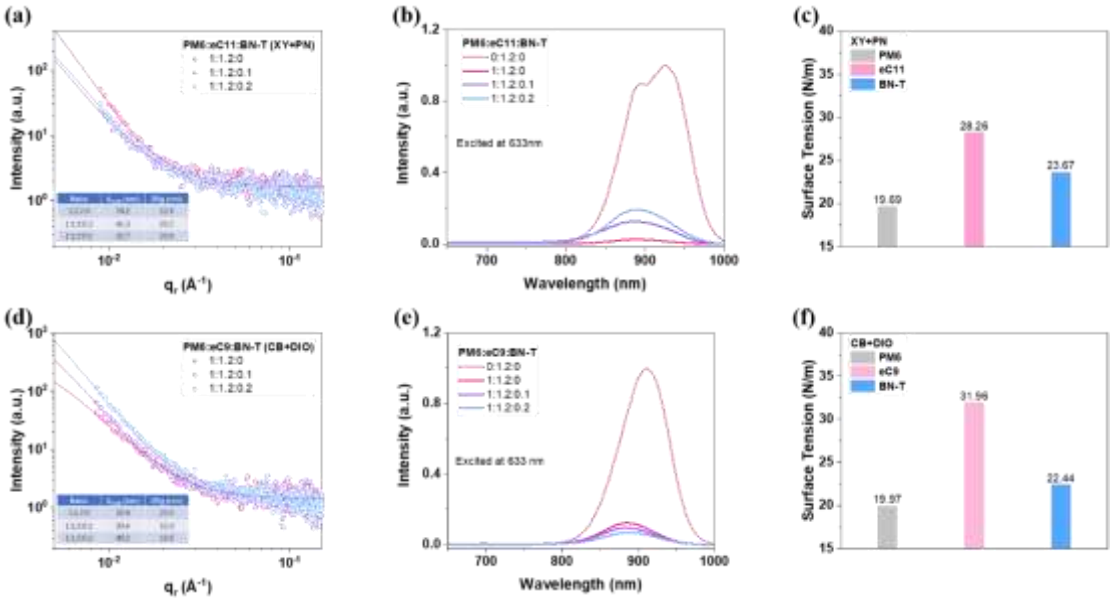

Figure 3. (a) In-plane GISAXS intensity plots and fitting curves for XY+PN processed PM6:eC11:BN-T systems. (b) PL spectra of eC11 neat film and blend films incorporating eC11. (c) Surface tension values of PM6, eC11 and BN-T films processed by XY+PN. (d) In-plane GISAXS intensity plots and fitting curves for CB+DIO processed PM6:eC9:BN-T systems. (e) PL spectra of eC9 neat film and blend films bearing eC9. (f) Surface tension values of PM6, eC9 and BN-T films processed by CB+DIO.

The phase separation length scales of targeted blends were measured by the grazing-incidence small-angle X-ray scattering (GISAXS) technique, using the Debye-Anderson-Brumberger equation as the fitting model.[59-62] **Figures 3a** and **3d** show the experimental results and fitting curves for PM6:eC11:BN-T (XY+PN) and PM6:eC9:BN-T (CB+DIO), respectively. **Figure S7** shows their two-dimensional patterns. The calculated domain sizes are also shown in the graphs (**Figure 3a** and **3d**), where $2Rg$ represents the length scale of the most crystalline material, and X_{DAB} is the size of the intermixing phase. Herein, eC11 and eC9 are of the strongest crystallinity in their own blends, because XY+PN processed eC11 neat film and CB+DIO processed eC9 neat film display foggy surfaces, meanwhile, XY+PN and CB+DIO processed

PM6 and BN-T films exhibit normal smooth surfaces. The PM6:eC11 binary film was evaluated pure acceptor phase with 12.6 nm length scale and an intermixing domain of 76.2 nm, suggesting efficient charge dissociation and extraction but potentially stronger bimolecular recombination. Then the optimal PM6:eC11:BN-T (1:1.2:0.1) blend exhibits a eC11 domain with a length scale of 25.2 nm and a mixed phase with a length scale of 41.3 nm, which potentially achieves the balance of efficient charge dissociation and transport. When the BN-Tamount increased to 0.2, the length scales of eC11 domain and mixed phase decline to 20.8 and 32.7 nm, respectively. **Figure 2b** shows a PL quenching comparison that verifies this conclusion, with the binary control film having the maximum quenching efficiency and the ternary target film having a lower value. The reduced phase separation is consistent with the BN-T's effect of alleviating the excessive J- aggregation of eC11. This change could facilitate the balance of charge generation and transport.

Next, we concentrated on the domain size change of CB+DIO processed system. PM6:eC9 based active layer was calculated to have a 22.6 nm pure acceptor phase and a 20.8 nm intermixing phase, implying a well-distributed film morphology. The optimal PM6:eC9:BN-T (1:1.2:0.1) exhibits a eC9 domain with a length scale of 15.4 nm, and a mixed phase of ~ 33.4 nm. The film achieves a more intermixing phase (49.2 nm) with a decreased pure acceptor domain of 10.8 nm when the BN-T fraction is 0.2. These results are displayed in **Figure 2d** and are consistent with the PL quenching efficiency comparison for each ratio depicted in **Figure 2e**. Afterwards, atomic force microscopy (AFM) studies were then employed to examine the surface morphological change of PM6:eC11:BN-T (XY+PN) and PM6:eC9:BN-T (CB+DIO), as depicted in **Figures S8** and **S9**. The observed variation tendencies of phase segregation in both series are in consistence with GISAXS technology based calculation.

To understand the morphology evolutions in this work, we performed miscibility analysis based on surface tension of each material. The water and ethylene glycol contact angles on films are displayed in **Figures S10** and **S11**. Surface tensions of PM6 films treated by XY+PN and CB+DIO are very comparable, however, surface tensions of BN-T neat films cast by two co-solvents are quite different, consistent with their

absorption profile changes. The surface tensions of eC11 cast by XY+PN and eC9 cast by CB+DIO are also obtained, and displayed in **Figures 3c** and **3f**. According to Flory-Huggins interaction theory and prior OSC studies, PM6 and eC9 tend to form well separated phases. The addition of BN-T can reduce phase separation, resulting in smaller crystallites and larger intermixing domains. This deduction can properly describe the role of BN-T in CB+DIO cast PM6:eC9 systems. However, the miscibility study fails in the prediction of XY+PN processed PM6:eC11:BN-T series, where PM6 and eC11 should also demonstrate significant phase separation in binary films. After the introduction of BN-T, ternary films should go through a process of reducing pure acceptor phase length scales and enlarging intermixing domain sizes. This prediction contradicts the experimental findings.

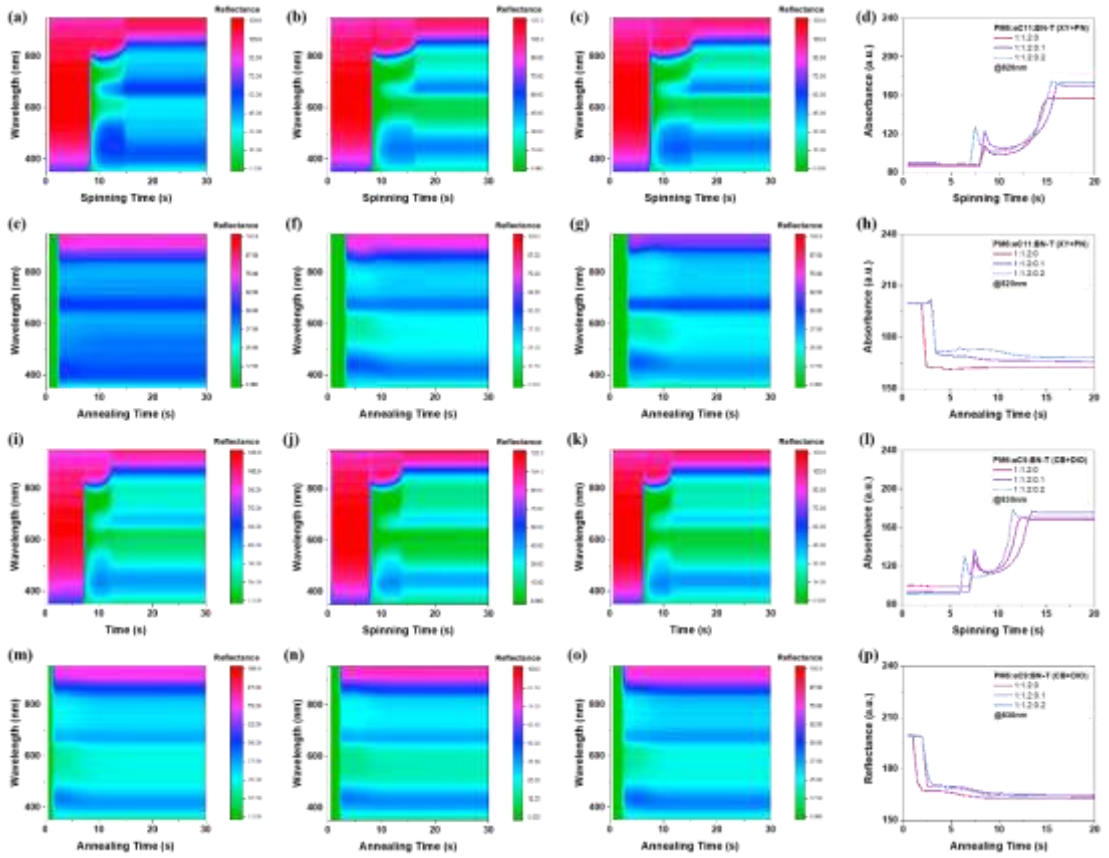

Figure 4. Contour maps of time-wavelength-reflection intensity for the spinning and annealing process. PM6:eC11:BN-T (XY+PN) spinning: (a) 1:1.2:0, (b) 1:1.2:0.1, and (c) 1:1.2:0.2; annealing: (e) 1:1.2:0, (f) 1:1.2:0.1, and (g) 1:1.2:0.2. PM6:eC9:BN-T (CB+DIO) spinning: (i) 1:1.2:0, (j) 1:1.2:0.1, and (k) 1:1.2:0.2; annealing: (m) 1:1.2:0, (n) 1:1.2:0.1, and (o) 1:1.2:0.2. Calculated time-resolved absorption intensity variations

for all blends at various position: (d) Spin of PM6:eC11:BN-T systems at 820 nm; (h) anneal of PM6:eC11:BN-T films at 820 nm; (l) Spin of PM6:eC9:BN-T systems at 830 nm; (p) anneal of PM6:eC9:BN-T films 830 nm.

In the following step, we use time-resolved reflectance measurement to understand the transition from solution to treated film(s), and the operating mode is depicted in **Figure S12**. The collected data are depicted as 2D contour maps, where colors represent the reflectance signal intensity at a specific time and wavelength; time-resolved absorbance at fixed wavelengths of the films was then extracted and derived. These results are all demonstrated in **Figure 4**. The aggregation durations of ternary films are shown to be longer than those of binary counterparts for XY+PN processed series by tracking absorbance at 820 nm, implying that the incorporation of BN-T inclusion retains more solvent(s), especially the higher boiling point one (PN). The solvent additive removal process can therefore be easily observed by screening the annealing induced absorption change (Figure 4h) for ternary blends: the absorption intensities went through a *ca.* 6-second drop, indicating the fast evaporation of high boiling point solvent additive PN.

The binary film, by contrast, displays a very short and vague stage of PN evaporation, implying the significantly lower PN retention after spinning therein. In view of the prolonged film drying time and solvent additive removal period, the incorporation of BN-T is believed to impede considerable PN evaporating during the spinning.[45] For this situation, the final morphology should be determined not only by the interaction of active materials, but also by the different evaporation processes of PN. CB+DIO processed eC9 based films were also investigated. According to **Figure 4l**, the longest aggregation time is achieved by the 1:1.2:0.1 ratio, which might partially explain its strongest π-π crystallinity, but the time differences are not equally significant. The time-dependent absorption intensities for eC9 in the films under thermal annealing (**Figure 4p**) exhibit highly similar profiles, implying the DIO removal processes are almost uniform. This phenomenon indicates that the DIO residual ratio in films is quite similar; in other words, adding BN-T does not effectively increase or decrease the content of DIO after spinning, and thus the morphology differences for this series may be

attributed primarily to the interaction of photoactive materials.

To further reveal BN-T's aggregation behavior coping with two co-solvents, the real-time reflectance spectra of its neat film's formation process were also tested, as shown in **Figure S13**. It can be easily observed that BN-T has a longer drying time during the spin casting in XY+PN co-solvent than in CB+DIO, which is consistent with the previous discussion. Meanwhile, the real-time observation of the thermal annealing process implies that more solvent was removed from XY+PN cast film than CB+DIO processed one, which also supports the aforementioned hypothesis. Moreover, we deployed Fourier-transform infrared (FT-IR) spectroscopy technology to gain a better understanding of the BN-T effect. **Figure S14** shows that the XY+PN cast film exhibits significant peaks from 750 to 800 cm-1, which reflect the substitution bonds of benzene, corresponding to PN. Meanwhile, other characteristic peaks show no differences. This result demonstrates that BN-T can retain significantly more PN in the film until thermal annealing is applied, hence substantiating the abovementioned supposition.

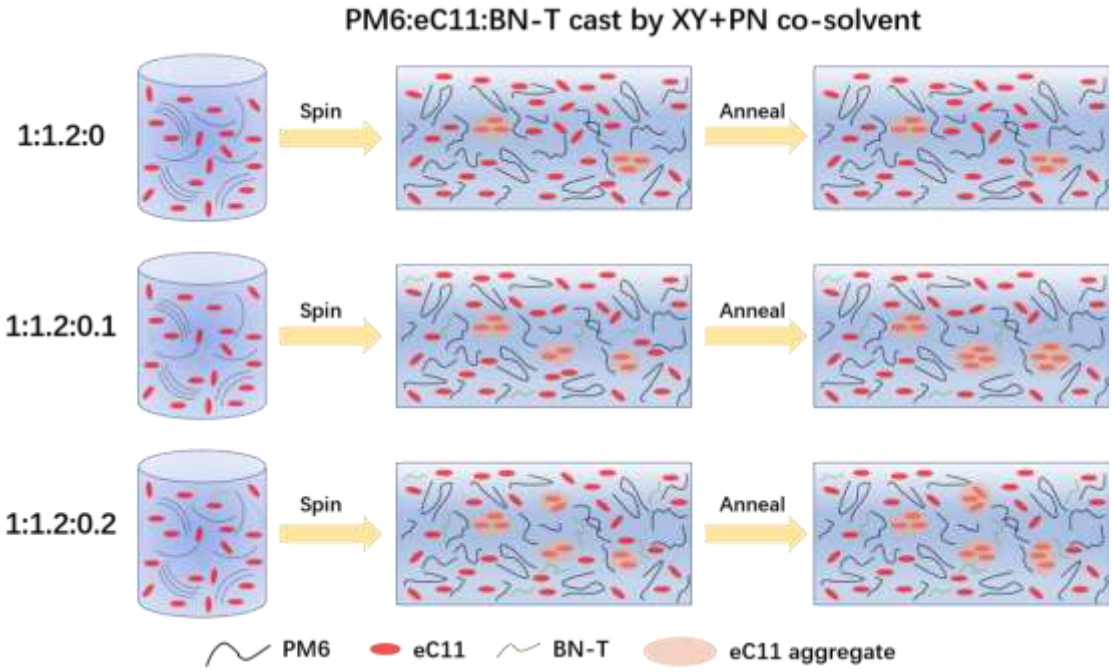

Figure 5. The schematic morphology evolution for XY+PN processed PM6:eC11:BN-T films of each weight ratio.

To demonstrate the morphology evolution in this work as clearly as possible, based on evidence obtained, a schematic diagram of PM6:eC11:BN-T (XY+PN) systems is

then presented as **Figure 5**. Previous time-resolved studies have shown that primary solvents such as CB, XY, and o-DCB are basically eliminated after spinning, leaving solvent additives such as DIO, PN, and 1-CN as the dominant liquid composition in films.[36] Herein, an extremely small quantity of PN was kept in the film for the binary system, resulting in a well-miscible donor-acceptor interpenetrating morphology. When 0.1 BN-T was included, PN continuously strengthen phase segregation, engendering more and larger pure eC11 domains. Increasing the BN-T's ratio to 0.2, the mixing domains were further reduced, enabling more pure acceptor phases. However, the length scales of acceptor phases are slightly smaller, probably because BN-T is highly amorphous in film. We attribute this intricate morphological evolution to a coupling and competition between improved phase segregation caused by the BN-T induced larger PN retention and the weakened segregation caused by the amorphous BN-T. This could also explain the subtle variation in crystallinity for PM6:eC11:BN-T films. As for the CB+DIO cast PM6:eC9:BN-T films, the introduction of BN-T has negligible impact upon the retention of solvent additive. As a result, the removal of DIO is expected to result in equal morphological changes during the cast and after treatment. As mentioned in the miscibility study, the main changes in their morphology are driven by the interaction of PM6, BN-T, and eC9. The intricate change in crystallinities observed here is consistent with our prior study based on an all-polymer system.[26]

Conclusion

In summary, cutting-edge efficiencies were first achieved for both non-halogenated and halogenated co-solvents processed ternary OSCs with amorphous polymer acceptor (BN-T). While a simple miscibility scenario enables a reasonable understanding of the morphological changes for PM6:eC9:BN-T blend films of different weight ratios cast from CB+DIO precursors, it fails in explaining XY+PN cast PM6:eC11:BN-T system behaviors. Time-resolved reflectance spectroscopy revealed that the abnormity is due to the new phenomenon that BN-T can remain more solvent additive in film, resulting in highly different evolution routes for morphology formation. This work provides a deeper understanding of the thin film morphology tuning effect of the ternary-

component strategy, emphasizes the role of co-solvent selection, and provides a new and facile in-situ characterization method to investigate the working mechanism when ex-situ observation results contradict the prediction of the popular miscibility analysis.

Author Contribution

Ruijie Ma: Conceptualization, Methodology, Investigation, Formal Analysis, Writing – Original Draft

Cenqi Yan: Investigation, Writing Review & Editing

Patrick Wai-Keung Fong: Software, Investigation

Jiangsheng Yu: Investigation

Heng Liu: Investigation

Junli Yin: Investigation

Jianhua Huang: Resources

Xinhui Lu: Resources

He Yan: Resources, Supervision

Gang Li: Resources, Supervision, Writing Review & Editing, Project Administration

Note

Authors declare no conflict of interest.

Acknowledgement

G. Li thanks the support from Research Grants Council of Hong Kong (GRF grant 15218517, CRF C5037-18G), National Science Foundation of China (NSFC 51961165102), Shenzhen Science and Technology Innovation Commission (Project No. JCYJ 20200109105003940), the Hong Kong Polytechnic University funds (Sir Sze-yuen Chung Endowed Professorship Fund (8-8480), RISE (CDA5), SAC5). H. Yan appreciates the support from the National Key Research and Development Program of China (No. 2019YFA0705900) funded by MOST. The Basic and Applied Basic Research Major Program of Guangdong Province (No. 2019B030302007), Guangdong-Hong Kong-Macao Joint Laboratory of Optoelectronic and Magnetic

Functional Materials (project number 2019B121205002), the Shen Zhen Technology and Innovation Commission (project number JCYJ20170413173814007, JCYJ20170818113905024), the Hong Kong Research Grants Council (Research Impact Fund R6021-18, collaborative research fund C6023-19G, project numbers 16309218, 16310019, and 16303917, RFS2021-6S05), Hong Kong Innovation and Technology Commission for the support through projects ITC-CNERC14SC01 and ITS/471/18), National Natural Science Foundation of China (NSFC, No. 91433202). R. Ma thanks the support from Hong Kong PhD Fellowship Scheme PF17-03929.

Reference

1. C. Li, J. Zhou, J. Song, J. Xu, H. Zhang, X. Zhang, J. Guo, L. Zhu, D. Wei, G. Han, J. Min, Y. Zhang, Z. Xie, Y. Yi, H. Yan, F. Gao, F. Liu and Y. Sun, *Nat. Energy*, 2021, **6**, 605-613.
2. Y. Cui, Y. Xu, H. Yao, P. Bi, L. Hong, J. Zhang, Y. Zu, T. Zhang, J. Qin, J. Ren, Z. Chen, C. He, X. Hao, Z. Wei and J. Hou, *Adv. Mater.*, 2021, **33**, 2102420.
3. L. Zhan, S. Li, Y. Li, R. Sun, J. Min, Z. Bi, W. Ma, Z. Chen, G. Zhou, H. Zhu, M. Shi, L. Zuo and H. Chen, *Joule*, DOI: 10.1016/j.joule.2022.02.001.
4. S. Bao, H. Yang, H. Fan, J. Zhang, Z. Wei, C. Cui and Y. Li, *Adv. Mater.*, 2021, **33**, 2105301.
5. L. Hong, H. Yao, Y. Cui, P. Bi, T. Zhang, Y. Cheng, Y. Zu, J. Qin, R. Yu, Z. Ge and J. Hou, *Adv. Mater.*, 2021, **33**, 2103091.
6. H. Meng, C. Liao, M. Deng, X. Xu, L. Yu and Q. Peng, *Angew. Chem. Int. Ed.*, 2021, **60**, 22554-22561.
7. S. Chen, L. Feng, T. Jia, J. Jing, Z. Hu, K. Zhang and F. Huang, *Sci. China Chem.*, 2021, **64**, 1192-1199.
8. L. Zuo, S. B. Jo, Y. Li, Y. Meng, R. J. Stoddard, Y. Liu, F. Lin, X. Shi, F. Liu, H. W. Hillhouse, D. S. Ginger, H. Chen and A. K. Y. Jen, *Nat. Nanotech.*, 2022, **17**, 53-60.
9. L. Liu, S. Chen, Y. Qu, X. Gao, L. Han, Z. Lin, L. Yang, W. Wang, N. Zheng, Y. Liang, Y. Tan, H. Xia and F. He, *Adv. Mater.*, 2021, **33**, 2101279.
10. M. Zhang, L. Zhu, G. Zhou, T. Hao, C. Qiu, Z. Zhao, Q. Hu, B. W. Larson, H. Zhu, Z. Ma, Z. Tang, W. Feng, Y. Zhang, T. P. Russell and F. Liu, *Nat. Commun.*, 2021, **12**, 309.
11. Y. Lin, Y. Firdaus, F. H. Isikgor, M. I. Nugraha, E. Yengel, G. T. Harrison, R. Hallani, A. El-Labban, H. Faber, C. Ma, X. Zheng, A. Subbiah, C. T. Howells, O. M. Bakr, I. McCulloch, S. D. Wolf, L. Tsetseris and T. D. Anthopoulos, *ACS Energy Lett.*, 2020, **5**, 2935-2944.
12. F. Liu, L. Zhou, W. Liu, Z. Zhou, Q. Yue, W. Zheng, R. Sun, W. Liu, S. Xu, H. Fan, L. Feng, Y. Yi, W. Zhang and X. Zhu, *Adv. Mater.*, 2021, **33**, 2100830.
13. X. Meng, K. Jin, Z. Xiao and L. Ding, 2021, **42**, 100501.
14. J. Qin, Q. Yang, J. Oh, S. Chen, G. O. Odunmbaku, N. A. N. Ouedraogo, C. Yang, K. Sun and S. Lu, *Adv. Sci.*, 2022, **n/a**, 2105347.
15. C. Cui and Y. Li, *Aggregate*, 2021, **2**, e31.
16. N. Gasparini, A. Salleo, I. McCulloch and D. Baran, *Nat. Rev. Mater.*, 2019, **4**, 229-242.
17. N. Y. Doumon, L. Yang and F. Rosei, *Nano Energy*, 2022, **94**, 106915.

18. X. Xu, Y. Li and Q. Peng, *Adv. Mater.*, 2021, **n/a**, 2107476.
19. R. Ma, T. Liu, Z. Luo, K. Gao, K. Chen, G. Zhang, W. Gao, Y. Xiao, T.-K. Lau, Q. Fan, Y. Chen, L.-K. Ma, H. Sun, G. Cai, T. Yang, X. Lu, E. Wang, C. Yang, A. K. Y. Jen and H. Yan, *ACS Energy Lett.*, 2020, **5**, 2711-2720.
20. H. Zhao, B. Lin, J. Xue, H. B. Naveed, C. Zhao, X. Zhou, K. Zhou, H. Wu, Y. Cai, D. Yun, Z. Tang and W. Ma, *Adv. Mater.*, 2022, **34**, 2105114.
21. B. Fan, W. Gao, Y. Wang, W. Zhong, F. Lin, W. J. Li, F. Huang, K.-M. Yu and A. K. Y. Jen, *ACS Energy Lett.*, 2021, **6**, 3522-3529.
22. R. Ma, K. Zhou, Y. Sun, T. Liu, Y. Kan, Y. Xiao, T. A. Dela Peña, Y. Li, X. Zou, Z. Xing, Z. Luo, K. S. Wong, X. Lu, L. Ye, H. Yan and K. Gao, *Matter*, 2022, **5**, 725-734.
23. L. Nian, Y. Kan, K. Gao, M. Zhang, N. Li, G. Zhou, S. B. Jo, X. Shi, F. Lin, Q. Rong, F. Liu, G. Zhou and A. K. Y. Jen, *Joule*, 2020, **4**, 2223-2236.
24. J. Qin, Z. Chen, P. Bi, Y. Yang, J. Zhang, Z. Huang, Z. Wei, C. An, H. Yao, X. Hao, T. Zhang, Y. Cui, L. Hong, C. Liu, Y. Zu, C. He and J. Hou, *Energy Environ. Sci.*, 2021, **14**, 5903-5910.
25. K. An, F. Peng, W. Zhong, W. Deng, D. Zhang, L. Ying, H. Wu, F. Huang and Y. Cao, *Sci. China Chem.*, 2021, **64**, 2010-2016.
26. T. Liu, T. Yang, R. Ma, L. Zhan, Z. Luo, G. Zhang, Y. Li, K. Gao, Y. Xiao, J. Yu, X. Zou, H. Sun, M. Zhang, T. A. Dela Peña, Z. Xing, H. Liu, X. Li, G. Li, J. Huang, C. Duan, K. S. Wong, X. Lu, X. Guo, F. Gao, H. Chen, F. Huang, Y. Li, Y. Li, Y. Cao, B. Tang and H. Yan, *Joule*, 2021, **5**, 914-930.
27. J. Wang, M. Zhang, J. Lin, Z. Zheng, L. Zhu, P. Bi, H. Liang, X. Guo, J. Wu, Y. Wang, L. Yu, J. Li, J. Lv, X. Liu, F. Liu, J. Hou and Y. Li, *Energy Environ. Sci.*, 2022, DOI: 10.1039/D1EE03673D.
28. X. Liao, Q. Xie, Y. Guo, Q. He, Z. Chen, N. Yu, P. Zhu, Y. Cui, Z. Ma, X. Xu, H. Zhu and Y. Chen, *Energy Environ. Sci.*, 2022, **15**, 384-394.
29. M. Jiang, H. Bai, H. Zhi, L. Yan, H. Y. Woo, L. Tong, J. Wang, F. Zhang and Q. An, *Energy Environ. Sci.*, 2021, **14**, 3945-3953.
30. Z. Zhang, D. Deng, Y. Li, J. Ding, Q. Wu, L. Zhang, G. Zhang, M. J. Iqbal, R. Wang, J. Zhang, X. Qiu and Z. Wei, *Adv. Energy Mater.*, 2022, **12**, 2102394.
31. Z. Chen, W. Song, K. Yu, J. Ge, J. Zhang, L. Xie, R. Peng and Z. Ge, *Joule*, 2021, **5**, 2395-2407.
32. Q. Liu, Y. Wang, J. Fang, H. Liu, L. Zhu, X. Guo, M. Gao, Z. Tang, L. Ye, F. Liu, M. Zhang and Y. Li, *Nano Energy*, 2021, **85**, 105963.
33. T. Zhang, C. An, Y. Cui, J. Zhang, P. Bi, C. Yang, S. Zhang and J. Hou, *Adv. Mater.*, 2022, **34**, 2105803.
34. R. Ma, J. Yu, T. Liu, G. Zhang, Y. Xiao, Z. Luo, G. Chai, Y. Chen, Q. Fan, W. Su, G. Li, E. Wang, X. Lu, F. Gao, B. Tang and H. Yan, *Aggregate*, 2021, **n/a**, e58.
35. M. Zhang, L. Zhu, T. Hao, G. Zhou, C. Qiu, Z. Zhao, N. Hartmann, B. Xiao, Y. Zou, W. Feng, H. Zhu, M. Zhang, Y. Zhang, Y. Li, T. P. Russell and F. Liu, *Adv. Mater.*, 2021, **33**, 2007177.
36. H. B. Naveed and W. Ma, *Joule*, 2018, **2**, 621-641.
37. J. Wang, C. Han, F. Bi, D. Huang, Y. Wu, Y. Li, S. Wen, L. Han, C. Yang, X. Bao and J. Chu, *Energy Environ. Sci.*, 2021, **14**, 5968-5978.
38. T. Liu, R. Ma, Z. Luo, Y. Guo, G. Zhang, Y. Xiao, T. Yang, Y. Chen, G. Li, Y. Yi, X. Lu, H. Yan and B. Tang, *Energy Environ. Sci.*, 2020, **13**, 2115-2123.
39. Z. Wang, K. Gao, Y. Kan, M. Zhang, C. Qiu, L. Zhu, Z. Zhao, X. Peng, W. Feng, Z. Qian, X.

Gu, A. K. Y. Jen, B. Z. Tang, Y. Cao, Y. Zhang and F. Liu, *Nat. Commun.*, 2021, **12**, 332.
40. H. Chen, R. Zhang, X. Chen, G. Zeng, L. Kobera, S. Abbrent, B. Zhang, W. Chen, G. Xu, J. Oh, S.-H. Kang, S. Chen, C. Yang, J. Brus, J. Hou, F. Gao, Y. Li and Y. Li, *Nat. Energy*, 2021, **6**, 1045-1053.
41. Y. Wang, X. Wang, B. Lin, Z. Bi, X. Zhou, H. B. Naveed, K. Zhou, H. Yan, Z. Tang and W. Ma, *Adv. Energy Mater.*, 2020, **10**, 2000826.
42. J. Yu, X. Liu, Z. Zhong, C. Yan, H. Liu, P. W. K. Fong, Q. Liang, X. Lu and G. Li, *Nano Energy*, 2022, **94**, 106923.
43. N. D. Eisenmenger, G. M. Su, G. C. Welch, C. J. Takacs, G. C. Bazan, E. J. Kramer and M. L. Chabinyc, *Chem. Mater.*, 2013, **25**, 1688-1698.
44. J. J. van Franeker, M. Turbiez, W. Li, M. M. Wienk and R. A. J. Janssen, *Nat. Commun.*, 2015, **6**, 6229.
45. Y. Li, H. Meng, T. Liu, Y. Xiao, Z. Tang, B. Pang, Y. Li, Y. Xiang, G. Zhang, X. Lu, G. Yu, H. Yan, C. Zhan, J. Huang and J. Yao, *Adv. Mater.*, 2019, **31**, 1904585.
46. Y. Cui, H. Yao, J. Zhang, K. Xian, T. Zhang, L. Hong, Y. Wang, Y. Xu, K. Ma, C. An, C. He, Z. Wei, F. Gao and J. Hou, *Adv. Mater.*, 2020, **32**, 1908205.
47. D. Wang, G. Zhou, Y. Li, K. Yan, L. Zhan, H. Zhu, X. Lu, H. Chen and C.-Z. Li, *Adv. Funct. Mater.*, 2021, **32**, 2107827.
48. X. Dong, Y. Jiang, L. Sun, F. Qin, X. Zhou, X. Lu, W. Wang and Y. Zhou, *Adv. Funct. Mater.*, 2021, **n/a**, 2110209.
49. Q. Zhao, H. Lai, H. Chen, H. Li and F. He, *J. Mater. Chem. A*, 2021, **9**, 1119-1126.
50. J. Ge, L. Hong, W. Song, L. Xie, J. Zhang, Z. Chen, K. Yu, R. Peng, X. Zhang and Z. Ge, *Adv. Energy Mater.*, 2021, **11**, 2100800.
51. S. Lee, D. Jeong, C. Kim, C. Lee, H. Kang, H. Y. Woo and B. J. Kim, *ACS Nano*, 2020, **14**, 14493-14527.
52. S. Zhang, L. Ye, H. Zhang and J. Hou, *Mater Today*, 2016, **19**, 533-543.
53. R. Ma, M. Zeng, Y. Li, T. Liu, Z. Luo, Y. Xu, P. Li, N. Zheng, J. Li, Y. Li, R. Chen, J. Hou, F. Huang and H. Yan, *Adv. Energy Mater.*, 2021, **11**, 2100492.
54. J. Rivnay, S. C. B. Mannsfeld, C. E. Miller, A. Salleo and M. F. Toney, *Chem. Rev.*, 2012, **112**, 5488-5519.
55. Z. Zhang, D. Deng, Y. Li, J. Ding, Q. Wu, L. Zhang, G. Zhang, M. J. Iqbal, R. Wang, J. Zhang, X. Qiu and Z. Wei, *Adv. Energy Mater.*, 2022, **12**, 2102394.
56. H. Sun, B. Liu, Y. Ma, J.-W. Lee, J. Yang, J. Wang, Y. Li, B. Li, K. Feng, Y. Shi, B. Zhang, D. Han, H. Meng, L. Niu, B. J. Kim, Q. Zheng and X. Guo, *Adv. Mater.*, 2021, **33**, 2102635.
57. Z. Peng, K. Xian, Y. Cui, Q. Qi, J. Liu, Y. Xu, Y. Chai, C. Yang, J. Hou, Y. Geng and L. Ye, *Adv. Mater.*, 2021, **33**, 2106732.
58. Z. Peng, L. Ye and H. Ade, *Materials Horizons*, 2022, **9**, 577-606.
59. X. Zhang, L. Qin, Y. Li, J. Yu, H. Chen, X. Gu, Y. Wei, X. Lu, F. Gao and H. Huang, *Adv. Funct. Mater.*, 2022, **n/a**, 2112433.
60. D. Wang, H. Liu, Y. Li, G. Zhou, L. Zhan, H. Zhu, X. Lu, H. Chen and C.-Z. Li, *Joule*, 2021, **5**, 945-957.
61. S. Jung, Y. Cho, S.-H. Kang, S.-J. Yoon and C. Yang, *Solar RRL*, 2022, **6**, 2100819.
62. R. Ma, T. Yang, Y. Xiao, T. Liu, G. Zhang, Z. Luo, G. Li, X. Lu, H. Yan and B. Tang, *Energy Environ. Mater.*, 2021, **n/a**.